J. Fluid Mech. (1998), *vol.* 364, *pp.* 325–347. Printed in the United Kingdom

Nonlinear free-surface flow due to an impulsively started submerged point sink

By MING XUE AND DICK K. P. YUE

Department of Ocean Engineering, Massachusetts Institute of Technology, Cambridge, MA 02139, USA

(Received 12 August 1997 and in revised form 9 February 1998)

The unsteady fully nonlinear free-surface flow due to an impulsively started submerged point sink is studied in the context of incompressible potential flow. For a fixed (initial) submergence h of the point sink in otherwise unbounded fluid, the problem is governed by a single non-dimensional physical parameter, the Froude number, $\mathscr{F} \equiv Q/4\pi(gh^5)^{1/2}$, where Q is the (constant) volume flux rate and g the gravitational acceleration. We assume axisymmetry and perform a numerical study using a mixed-Eulerian–Lagrangian boundary-integral-equation scheme. We conduct systematic simulations varying the parameter $\mathscr{F}$ to obtain a complete quantification of the solution of the problem. Depending on $\mathscr{F}$, there are three distinct flow regimes: (i) $\mathscr{F} < \mathscr{F}_1 \approx 0.1924$ – a 'sub-critical' regime marked by a damped wave-like behaviour of the free surface which reaches an asymptotic steady state; (ii) $\mathscr{F}_1 < \mathscr{F} < \mathscr{F}_2 \approx 0.1930$ – the 'trans-critical' regime characterized by a reversal of the downward motion of the free surface above the sink, eventually developing into a sharp upward jet; (iii) $\mathscr{F} > \mathscr{F}_2$ – a 'super-critical' regime marked by the cusp-like collapse of the free surface towards the sink. Mechanisms behind such flow behaviour are discussed and hydrodynamic quantities such as pressure, power and force are obtained in each case. This investigation resolves the question of validity of a steady-state assumption for this problem and also shows that a small-time expansion may be inadequate for predicting the eventual behaviour of the flow.

1. Introduction

We consider the incompressible irrotational axisymmetric flow caused by a point sink beneath a free surface. This is a problem of fundamental scientific interest and has engineering importance in applications such as optimal pumping from storage tanks, ocean thermal power plant, cooling and solar ponds, as well as water quality control in reservoirs and lakes. Because of this, the fluid 'withdrawal' problem has been the subject of many investigations in recent years.

Largely because of analytical and computational simplification, most of the studies are for the two-dimensional case assuming steady flow (Peregrine 1972; Vanden-Broeck, Schwartz & Tuck 1987; Tuck & Vanden-Broeck 1984; Sahin & Magnuson 1984; Hocking 1985, 1988; Collings 1986; Vanden-Broeck & Keller 1987; King & Bloor 1988; Mekias & Vanden-Broeck 1989, 1991, 1993). For infinite depth, stagnation-point solutions, those characterized by a stagnation point at the free surface directly above the sink, are found for Froude number $\mathscr{F}$ (based on the volume flux rate and submergence) below a critical value. Above this value, steady-state solutions

have not been found, except for a cusp solution (the free-surface profile is a downward facing cusp with its tip above the sink) at a unique super-critical value of $\mathscr{F}$.

A notable exception to these steady solutions is Tyvand (1992) who focused on the initial evolution of the free surface for the two-dimensional problem using a small-time expansion. Arguing that nonlinear free-surface effects are exactly cancelled by gravitational effects for a particular Froude number, he finds the critical value of $\mathscr{F} \equiv Q/2\pi(gh^3)^{1/2} = 1/3$ for the formation of a centre dip, where Q is the volume flux rate of the sink, h its submergence with respect to the far-field/initial free surface, and g the gravitational acceleration. This value is appreciably lower than the upper limit of $\mathscr{F} = 1.42$ of Hocking & Forbes (1991) based on a steady-state analysis, which, as pointed by Tyvand, shows that the unsteady problem offers new insight into its steady counterpart.

Investigations of the three-dimensional problem are fewer and more recent with the exception of linear analyses (e.g. Wehausen & Laitone 1960) and experiments (e.g. Lubin & Springer 1967; Miloh & Tyvand 1993). The salient feature of the experimental observations is the formation of a dip on the surface above a critical Froude number. Assuming steady state and a stagnation point at the surface above the sink, Forbes & Hocking (1990) used a boundary-integral-equation (BIE) computation as well as a small-Froude-number analysis to show that such a steady stagnation-point solution exists for small Froude numbers, in this case, $\mathscr{F} \equiv Q/4\pi(gh^5)^{1/2} < 0.509$. Above this value of $\mathscr{F}$, their calculation fails to give a steady-state solution. This, however, does not rule out unsteady/steady solutions below/above this value. Whether the unsteady withdrawal flow with a cusp pointing towards the sink is the only permissible outcome for large Froude number, in contrast to the corresponding two-dimensional problem (where a steady cusp-type flow exists even at infinite Froude number), remains unclear.

Zhou & Graebel (1990) perform numerical simulations of drainage from a cylindrical basin using a nonlinear axisymmetric BIE method. Their results for the unsteady problem show two different phenomena depending on the drain rate. For relatively large Q, a dip forms at centre of the free surface which is rapidly drawn into the drain. For small Q, they observe an upward jet depending on the drain size. In their problem, the Froude number is defined with respect to the tank radius. Since this is not the (only) physically important parameter, the precise dependence on $\mathscr{F}$ for this problem is not established.

More recently, Miloh & Tyvand (1993) extend the small-time perturbation analysis of Tyvand (1992) to axisymmetric flow and identify the corresponding critical Froude number to be $\mathscr{F} = 15^{-1/2} \approx 0.258$. Presumably, a dip forms on the free surface and eventually collapses towards the sink only for $\mathscr{F}$ greater than this value. This analysis depends only on the third-order (leading order of gravitational effect) time derivative of the centre surface elevation at time $t = 0$ and its validity for the long-time evolution of the actual physical problem is unclear.

In this paper, we consider the unsteady fully nonlinear free-surface flow above a submerged (three-dimensional) point sink started abruptly from rest to a constant volumetric withdrawal rate Q. The problem is governed by a single dimensionless physical parameter, the Froude number $\mathscr{F} \equiv Q/4\pi(gh^5)^{1/2}$, where h is the initial/far-field submergence and g the gravitational acceleration. We computationally map out the entire solution of the problem systematically varying $\mathscr{F}$. The computational method we employ is a fully nonlinear mixed Eulerian–Lagrangian (MEL) approach. We assume axisymmetry, and for the solution of the field equation we use an axisymmetric (ring-source) BIE technique (Dommermuth & Yue 1987). The paper is

organized as follows: the initial-boundary-value problem is stated in §2. The MEL axisymmetric BIE computational method, which follows closely that of Dommermuth & Yue (1987), is outlined also in §2 for completeness. Section 3 contains detailed validation of the computational method which is important to support the results which are presented in §4. We conclude with a summary and discussion in §5 where we compare our findings with existing results.

2. Problem statement and solution method

We consider a point sink with an initial (quiescent) submerged depth h below a free surface in an otherwise unbounded fluid. At initial time $t = 0$, the sink is turned on abruptly from zero to a constant volumetric flow rate Q. For simplicity, we choose time, length and mass units such that the depth h, the gravitational acceleration g, and the fluid density ρ are all unity. In the context of inviscid, irrotational, incompressible flow and ignoring surface tension, the problem is governed by a single physical parameter, the Froude number:

$$\mathscr{F} \equiv Q/4\pi(gh^5)^{1/2}. \tag{1}$$

We further assume that the flow is axisymmetric and non-rotating (cf. Monismith, McDonald & Imberger 1993). The resulting potential flow is described by a velocity potential $\phi(\boldsymbol{x}, t)$ with the fluid velocity given by $\boldsymbol{v} = \nabla\phi$. Inside the fluid domain $V(t)$, ϕ satisfies the Laplace equation

$$\nabla^2\phi = 0 \quad \text{in} \quad V(t). \tag{2}$$

On the free surface $F(\boldsymbol{x}, t)$, the kinematic and dynamic (assuming zero atmospheric pressure) boundary conditions in Lagrangian forms are

$$\frac{\mathrm{D}\boldsymbol{x}}{\mathrm{D}t} = \nabla\phi \quad \text{on} \quad F(\boldsymbol{x}, t), \tag{3}$$

$$\frac{\mathrm{D}\phi}{\mathrm{D}t} = -gz + \tfrac{1}{2}|\nabla\phi|^2 \quad \text{on} \quad F(\boldsymbol{x}, t), \tag{4}$$

where the vertical coordinate z is positive up, and $z = 0$ is the undisturbed free surface. At large depth, the velocity must vanish, $|\nabla\phi| \to 0$, $z \to -\infty$. For computations, the domain is simply closed at some large (constant) depth B: $z = -H$ with the condition

$$\frac{\partial\phi}{\partial z} = 0 \quad \text{on} \quad B\text{: } z = -H,\ H \gg 1. \tag{5}$$

Finally, we specify zero initial conditions and a suitable far-field condition:

$$\phi \to 0 \quad \text{as} \quad |\boldsymbol{x}| \to \infty,\ t < \infty. \tag{6}$$

For numerical solution of the initial-boundary-value problem, we adopt the fully nonlinear axisymmetric MEL method of Dommermuth & Yue (1987). In order to achieve long-time simulations, in that method, the far-field condition (6) is satisfied by matching the fully nonlinear inner MEL solution to a general time-dependent linearized outer wave field at a fixed radius on a matching cylinder M: $r = A$. Since the far-field wave amplitude must necessarily decay with radius in three dimensions, for a suitably chosen matching radius A (based on nonlinearity only), fully nonlinear (inner) simulations can be carried indefinitely in time (cf. Dommermuth & Yue 1987). This is especially important for the present problem where the approach to asymptotic steady state (or not) is a central question.

In the MEL approach, the boundary-value problem at each time step is solved using a boundary-integral method. From (2), the Green identity gives

$$\alpha(\boldsymbol{x},t)\phi(\boldsymbol{x},t) = \iint_{S(t)} \left[\frac{\partial\phi(\boldsymbol{x}',t)}{\partial n'} - \phi(\boldsymbol{x}',t)\frac{\partial}{\partial n'}\right]\frac{1}{R}\,\mathrm{d}S' + \frac{Q}{|\boldsymbol{x}-\boldsymbol{x}_{sink}|}, \tag{7}$$

where $\alpha(\boldsymbol{x})$ is the included solid angle at $\boldsymbol{x}$, $R = |\boldsymbol{x}-\boldsymbol{x}'|$ and $S(t) = \overline{F}\cup B\cup M$, with overbar denoting that portion of the surface enclosed by M. Note that in (7), the singularity at the sink, $\boldsymbol{x} = \boldsymbol{x}_{sink}$, of strength Q is already extracted.

Assuming axisymmetry, (7) can be integrated in θ' to yield a boundary integral in the $(r,\,z)$-plane:

$$\alpha(r,z,t)\phi(r,z,t) = Q\left(\frac{1}{d}+\frac{1}{d^*}\right) + \int_{\partial S(t)} r'\left[\frac{\partial\phi(r',z',t)}{\partial n'} - \phi(r',z',t)\frac{\partial}{\partial n'}\right] \times \left[G(r,z;r',z') + G(r,z;r',-z'-2H)\right]\mathrm{d}l'. \tag{8}$$

In the above, the line integral is along the trace $\partial S = \overline{\partial F}\cup\partial M$ of $\overline{F}\cup M$ in the $(r,\,z)$-plane; the bottom B is eliminated in favour of the image Green function with respect to the bottom $z=-H$; and $d = [(z+h)^2+r^2]^{1/2}$, $d^* = [(z+2H-h)^2+r^2]^{1/2}$. The Rankine ring-source Green function G is given by

$$G(r,z;r',z') = \int_0^{2\pi}\frac{\mathrm{d}\theta'}{R} = \frac{4}{\rho^*}K\left(1-\frac{\rho^2}{\rho^{*2}}\right), \tag{9}$$

where $\rho = [(z-z')^2+(r-r')^2]^{1/2}$, $\rho^* = [(z-z')^2+(r+r')^2]^{1/2}$, and K is the complete elliptic integral of the first kind.

In (8), neither ϕ nor $\partial\phi/\partial r$ on ∂M are *a priori* known in general. The transient history of the potential and the normal derivative of any linear wave field $\tilde{\phi}$ outside a closed surface M are however related, say

$$\tilde{\phi}\big|_M = \mathscr{H}\left.\frac{\partial\tilde{\phi}}{\partial n}\right|_M, \tag{10}$$

where $\mathscr{H}$ is a known spatial and temporal (convolution) integral operator (depending only on M) given in terms of (say) the transient free-surface Green function. Equation (10) together with the matching conditions on M:

$$\phi = \tilde{\phi} \quad\text{and}\quad \frac{\partial\phi}{\partial n} = \frac{\partial\tilde{\phi}}{\partial n} \quad\text{on}\quad M; \tag{11}$$

provide the necessary closure for the integral equation (8), and the solution is complete. Details can be found in Dommermuth & Yue (1987) where the validity and efficacy of this matching scheme are demonstrated. These are also verified directly for the present problem by comparing results obtained using different values of the matching radius A (see e.g. figure 1).

For the solution of (8) (with (10) and (11)), the trace $\partial S(t)$ is approximated by cubic splines over (Lagrangian) nodes, and ϕ and ϕ_n are represented by linear basis functions based on arclength between adjacent nodes. To maximize stability of the time integration, for which we employ a consistent fourth-order Runge–Kutta scheme, the nodes on the free surface are maintained at equal arclength spacing via a regridding procedure after each time step. To track the rapid cusp-like development of the free surface, the method of Dommermuth & Yue (1987) is improved by introducing dynamic time stepping based on a Courant criterion in terms of panel

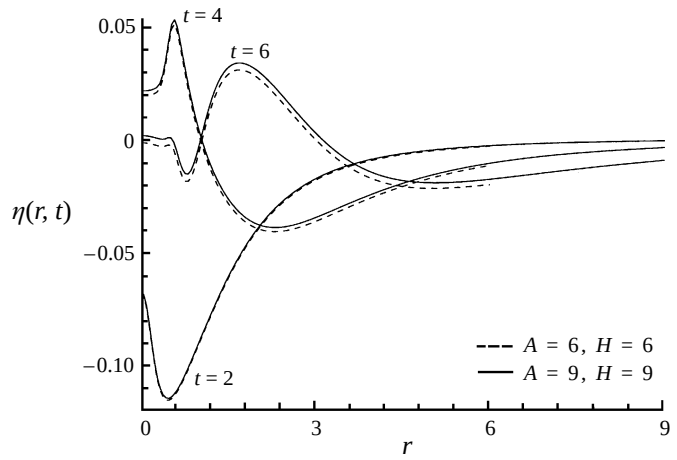

FIGURE 1. Free-surface profiles at different times for different matching radii A and computational depth H for the case $\mathscr{F} = 0.1$ ($\Delta\ell = 0.05$). The horizontal and vertical scales are different (the sink is at $z = -1$).

					$\eta(0,t)$			
A	H	Δl	Δt_{max}	Δt_{min}	$t = 0.48$	0.96	1.12	1.61
6	6	0.050	0.040	0.001	−0.0962	−0.1619	−0.1690	−0.1339
6	6	0.025	0.016	0.001	−0.0962	−0.1620	−0.1691	−0.1340
6	6	0.100	0.064	0.001	−0.0964	−0.1618	−0.1687	−0.1335
9	9	0.050	0.032	0.001	−0.0961	−0.1615	−0.1685	−0.1331
4	4	0.040	0.016	0.001	−0.0968	−0.1632	−0.1706	−0.1362

TABLE 1. Sample convergence results for the case of $\mathscr{F} = 0.1$.

size and the maximum instantaneous Lagrangian velocity. In theory, a small-time asymptotic expansion (cf. Miloh & Tyvand 1993) can be used to initiate the impulsive start. This is not found to be necessary in the present simulations.

3. Validation of the computational method

The computational method for this problem is validated systematically. A typical result is shown in table 1 for $\mathscr{F} = 0.1$ for the centreline surface elevation $\eta(r = 0, t)$, where we vary the (initial) panel (segment) length $\Delta\ell$, the depth of the computational domain H, the matching radius A, and the maximum and minimum time-step sizes, Δt_{max} and Δt_{min}, which are the upper and lower bounds of the time step Δt in the dynamic time integration scheme. (In all cases, the Courant condition derived from linearized free-surface conditions for the fourth-order Runge–Kutta scheme, $\Delta t^2 \leqslant 8\Delta\ell/\pi g$, is satisfied.)

Systematic tests such as these confirm the generally quadratic and fourth-order convergence rates of the absolute error with $\Delta\ell$ and Δt respectively. Table 1 also shows that a matching radius of $A = 6$ and a computational depth of $H = 6$ (to represent effective deep water) are sufficient. Figure 1 plots the free-surface profiles for $A, H = 6$ and 9 respectively at several time instants. Of special note is the absence of any reflection at the matching boundary $r = A$.

Based on these and similar test for the full range of $\mathscr{F}$ we consider, we choose for all our computations: $\Delta\ell$=0.05; $\Delta t_{max} = 0.032$; $\Delta t_{min} = 0.001$; $A = 6$; and $H = 6$. The expected error in the free-surface elevation is less than $O(1\%)$ in all cases.

All the computations are also checked for volume conservation:

$$\int\int_{\overline{F}} \frac{\partial \phi}{\partial n}\, \mathrm{d}S + \int\int_{M} \frac{\partial \phi}{\partial n}\, \mathrm{d}S = -Q, \tag{12}$$

and energy conservation:

$$\tfrac{1}{2}\rho Q \frac{\partial}{\partial t}\left[\phi - \frac{Q}{4\pi|\boldsymbol{x}-\boldsymbol{x}_{sink}|}\right]_{\boldsymbol{x}_{sink}} = \frac{\mathrm{d}}{\mathrm{d}t}\left[\int\int_{\overline{F}\cup M} \frac{\rho}{2}\phi\frac{\partial \phi}{\partial n}\, \mathrm{d}S + \int\int_{\overline{F}} \frac{\rho}{2} g z^2 n_z\, \mathrm{d}S\right] - \int\int_{M} \rho \frac{\partial \phi}{\partial t}\frac{\partial \phi}{\partial n}\, \mathrm{d}S. \tag{13}$$

In (13), the left-hand side is associated with the disturbance flow net of the sink flow, which is non-singular. This is the sum of the rate of energy input and the rate of work done by the sink, and equals half the rate of work done (i.e. power) by the sink. The first term on the right-hand side represents the rate of increase of kinetic and potential energy in the fluid volume $\overline{V}$; and the last term represents the rate of energy flux across the matching boundary M. Note that the kinetic energy introduced into the fluid at the initial instant is inversely proportional to the (small) dimension of the sink, and in the present case of an idealized point sink, is in theory unbounded. Nevertheless, for finite time thereafter, the power associated with the draining is well defined and does not depend on the (small) sink dimension. For all the runs, volume is typically conserved to within 0.001% and energy conservation (13) maintained to less than 1%.

4. Results

We perform a systematic computational investigation varying the only physical parameter $\mathscr{F}$ to provide a complete quantification of the solution of this problem. Careful search over the entire range of $\mathscr{F} > 0$ reveals three distinct flow regimes corresponding to: (i) $\mathscr{F} < \mathscr{F}_1$: sub-critical case; (ii) $\mathscr{F}_1 < \mathscr{F} < \mathscr{F}_2$: trans-critical case; and (iii) $\mathscr{F} > \mathscr{F}_2$: super-critical case; with $\mathscr{F}_1 \approx 0.1924$ and $\mathscr{F}_2 \approx 0.1930$. These values are obtained with (final) Froude number increments $\delta\mathscr{F} \ll 10^{-4}$ and are not affected when space–time discretizations are further refined. The solutions in these three regimes are described separately below.

4.1. *Sub-critical regime: $\mathscr{F} < \mathscr{F}_1 \approx 0.1924$*

In this sub-critical regime, the flow is marked by a damped wave-like behaviour of the free surface which eventually tends to an asymptotic steady state. A typical sub-critical result for $\mathscr{F} = 0.1$ is shown in figure 2 for the free-surface profiles at different times. The free surface near the origin initially goes down, reaches a minimum value, then rises and then settles towards an asymptotic value in an oscillatory manner emitting outwardly propagating radial waves in the process. Note that with the use of the matching boundary, we are able to continue simulations to well beyond $O(10)$ characteristic time (limited only by computational effort).

The wave-like behaviour is better seen in the time-histories of the free-surface elevation at specific radii (figure 3). At each r, the free surface behaves like a damped oscillator, eventually reaching an asymptotic steady state. That the time for steady

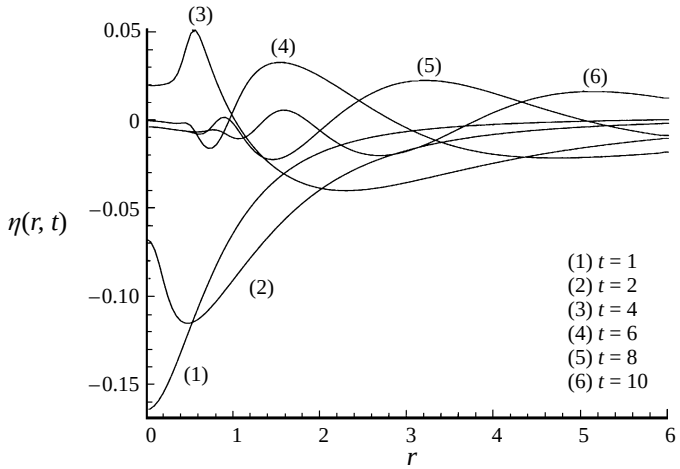

FIGURE 2. Free-surface profiles at different times for sub-critical $\mathscr{F} = 0.1$. The horizontal and vertical scales are different (the sink is at $z = -1$).

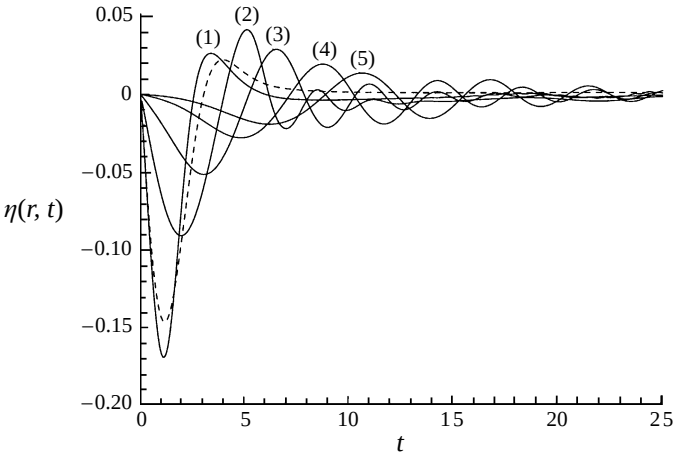

FIGURE 3. Time histories of the free-surface elevation for sub-critical $\mathscr{F} = 0.1$ at different radii curve (1) $r = 0$; (2) 1; (3) 2; (4) 4; (5) 6. The dashed line is the elevation at $r = 0$ from linear theory according to equation (15).

state to be reached increases with distance from the centre is evident from figure 3. It is shown more clearly in a space–time ('waterfall') plot of the surface elevation (figure 4) where there is a discernible receding wave front, behind which an asymptotic steady state establishes.

A perhaps more convincing proof that an asymptotic steady state is reached is a plot of the volume flux rate across a fixed radius. This is shown in figure 5 for $r = 1$. After about $t \sim 10$, the flux rate reaches a constant value of close to Q indicating that steady state is reached for $r < 1$. A plot of the instantaneous velocity field helps explain this type of behaviour. This is shown in figure 6 for $t = 2$, which shows the existence of a stagnation point on the centreline above the sink, and a dividing streamline terminating at the stagnation point. As steady state is reached, the dividing streamline no longer moves and the flux into the sink comes completely from flow below this streamline.

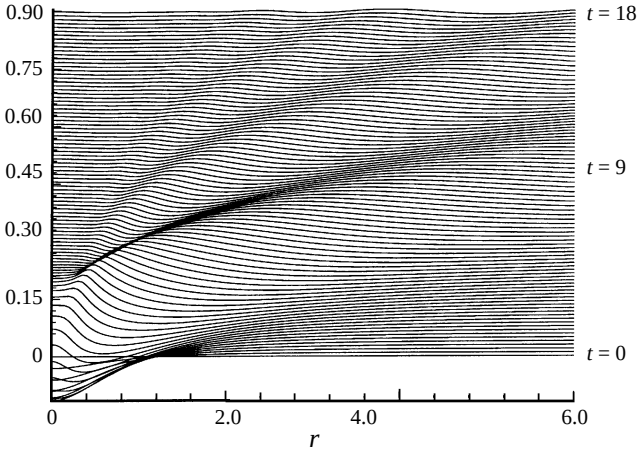

FIGURE 4. Space–time plot of the free-surface profiles $\eta(r, t)$ for sub-critical $\mathscr{F} = 0.1$. Time increment between two successive free-surface profiles is $\Delta t = 0.2$.

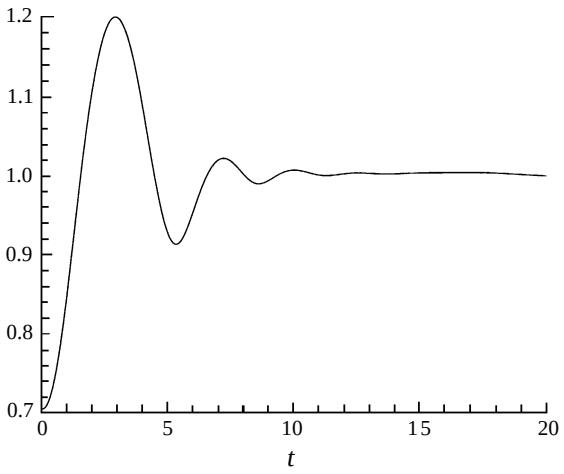

FIGURE 5. Volume flux rate (normalized by Q) across $r = 1$ as a function of time, for sub-critical $\mathscr{F} = 0.1$.

From figure 3 (for example, for $r = 1$ and 2, asymptotic steady states are reached at $t \simeq 14$ and 18 respectively), and the slope of the receding front in figure 4, one estimates that the radius below which an asymptotic steady state is reached increases with time with a group velocity of $C_g \simeq 0.25$. From figure 4, the corresponding wavelength can also be estimated to be $\lambda \simeq 1.6$. This is in good agreement with the linearized (two-dimensional for reasonably large r) dispersion relation $C_g \simeq 0.2\lambda^{1/2}$ and is consistent with diminishing nonlinear effects away from the centre.

For sufficiently small $\mathscr{F}$, one may apply linearized free-surface boundary conditions throughout, and the solution of the linearized problem can be written in closed form (cf. Wehausen & Laitone 1960):

$$\phi(r, z, t) = \mathscr{F}\left(\frac{1}{|\boldsymbol{x} - \boldsymbol{x}_{sink}|} + \frac{1}{|\boldsymbol{x} - \boldsymbol{x}^*_{sink}|}\right) - 2\mathscr{F}\int_0^\infty \cos(k^{1/2}t)\mathrm{e}^{k(z-1)}J_0(kr)\,\mathrm{d}k \qquad (14)$$

where $\boldsymbol{x}^*_{sink}$ is the image point of the sink about the undisturbed free surface. The

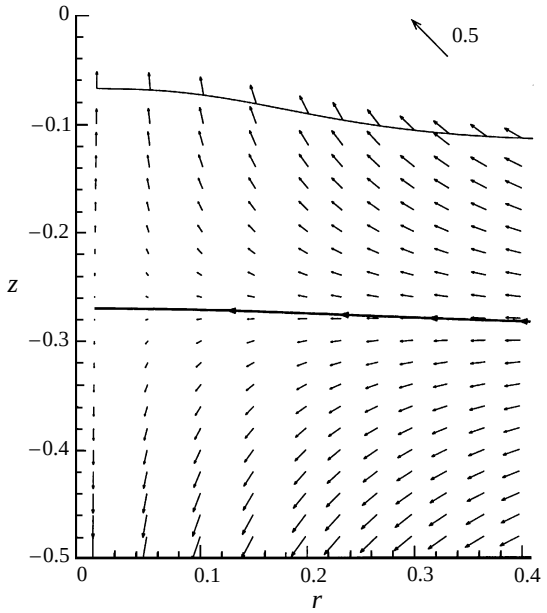

FIGURE 6. Velocity field for sub-critical $\mathscr{F} = 0.1$ at $t = 2$. The dividing streamline terminating at the stagnation point near $(0, -0.27)$ is also plotted. The vertical and horizontal scales are equal (the sink is at $(0, -1)$). Note that for clarity the left-hand axis of the figure is displaced from $r = 0$. A reference vector is given above.

corresponding free-surface elevation is

$$\eta(r,t) = -2\mathscr{F}\int_0^\infty k^{1/2}\sin(k^{1/2}t)\mathrm{e}^{-k}J_0(kr)\,\mathrm{d}k. \tag{15}$$

It is easy to see (e.g. using integration by parts) that the integral terms in (14) and (15) vanish with increasing time for any finite r so that the linearized result does predict asymptotic steady state. Specifically, from (15), we obtain the behaviour for the free-surface elevation, say at the origin: $\eta(0,t)$. This is plotted in figure 3. The surface elevation first decreases to reach its lowest level $\eta_{min} \approx -1.466\mathscr{F}$ at $t = 1.191$, then reverses direction to reach its highest (positive) value $\eta_{max} \approx 0.220\mathscr{F}$ at $t = 3.911$, after which it decreases monotonically in time to zero (the far-field level). This is different from that of the corresponding linearized solution for a two-dimensional sink flow. In the latter case, the elevation first drops to its lowest level (at $t = 1.848$) then reverses direction to monotonically reach the far-field level without ever becoming positive.

Although linear theory predicts the asymptotic steady state, it should be noted that the sub-critical regime extends beyond where linear theory is valid. In some sense, the linear prediction of the steady state is a trivial one at least in the limiting case of $\mathscr{F} = 0$ – the sink and its image with the undisturbed free surface being a plane of symmetry. In fact, figure 3 agrees with (15) well (say with maximum normalized error of 2%) only for $\mathscr{F}$ less than about 0.02 (see figure 15).

4.2. *Super-critical regime: $\mathscr{F} > \mathscr{F}_2 \approx 0.1930$*

For Froude number greater than a critical value of $\mathscr{F}_2 \approx 0.1930$, the solution is characterized by a rapid cusp-like collapse of the free surface towards the sink. The decrease of the surface elevation is everywhere monotonic in time. We are able to

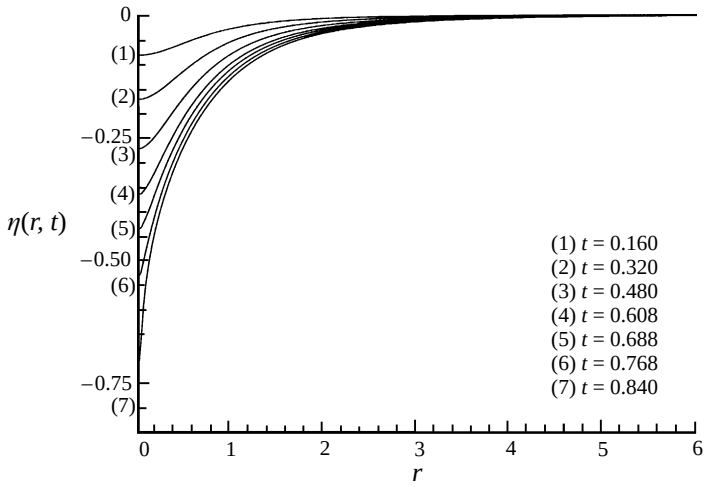

FIGURE 7. Free-surface profiles at different times for super-critical $\mathscr{F} = 0.24$. The horizontal and vertical scales are different (the sink is at $z = -1$).

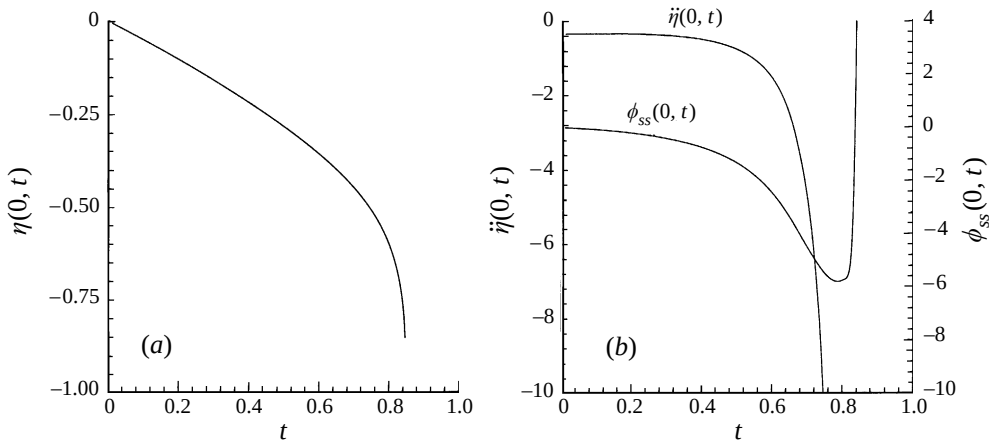

FIGURE 8. Time evolution of (a) the centreline free-surface elevation $\eta(0,t)$, and (b) acceleration $\ddot{\eta}(0,t)$ and strain rate $\phi_{ss}(0,t)$ (s is arclength) for super-critical $\mathscr{F} = 0.24$.

compute well after the cusp has developed, limited by the spatial discretizations and minimum temporal increment we use. Eventually, as the free surface approaches the sink, the velocity asymptotically develops a inverse square singularity, and the simulations finally break down.

Figure 7 shows typical super-critical results for the case of $\mathscr{F} = 0.24$ for the instantaneous free-surface profiles $\eta(r,t)$ at different times of the development of the centre dip. The decrease in elevation is everywhere monotonic in time and monotonically increasing with decreasing radial distance for all time, eventually developing a cusp-like profile. Figure 8 plots the time evolution of the free-surface elevation and the acceleration directly above the sink. The rapidly increasing (downward) acceleration towards the sink eventually reaches very large magnitudes. The super-critical regime is the only regime for this problem where the downward acceleration exceeds gravitational acceleration ($g = 1$) during the fall of the free surface.

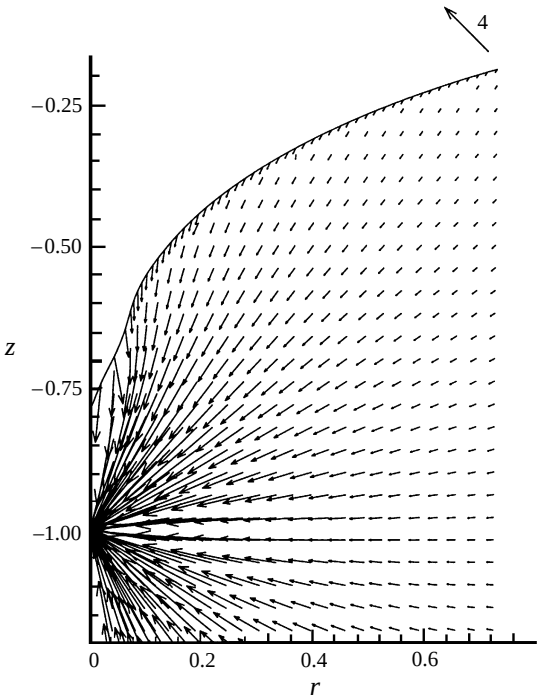

FIGURE 9. Velocity field for super-critical $\mathscr{F} = 0.24$ at $t = 0.84$. Note the sink is at $z = -1$ and the vertical and horizontal scales are equal. A reference vector is given.

The solution behaviour for the super-critical regime can be expected from physical arguments at least in the limiting case. As $\mathscr{F}$ increases, the effect of the sink eventually dominates that of gravity and the solution then resembles that of a single point sink. This general feature is shown in the velocity field plot in the final stage of the dip formation ($t = 0.84$) for $\mathscr{F} = 0.24$ (figure 9). The surface velocities at the centre are dominant while those away from the centre are small, consistent with the rapid formation of the dip observed for example by Lubin & Springer (1967). At this stage of the evolution, the entire flow field resembles that due to a pure sink-induced flow at $(0, -1)$ with a dividing streamline approximately aligned with $z = -1$.

The overall dynamics can be elucidated by examining the pressure field (e.g. Zhou & Graebel 1990). Figure 10 plots the pressure contours at three instants corresponding respectively to early, intermediate and late stages of the free-surface collapse. At an early time (figure 10*a*), there are two zero pressure lines: the free surface, and another line inside the fluid domain around the sink. There exist then a region of positive pressure and a pressure maximum above the sink below the free surface. As time progresses (figure 10*b*), the interior zero-pressure line connects to the free surface, eliminating the positive pressure region above the sink. The pressure gradient on the centerline above the sink obtains a single sign (directed from the sink to the free surface). This pressure gradient increases rapidly as the free surface drops closer to the sink (figure 10*c*), and the free surface eventually develops a sharp dip towards the sink.

We remark finally that although the free surface experiences acceleration into the fluid much greater than gravity ($g = 1$) in the development of the downward dip (cf.

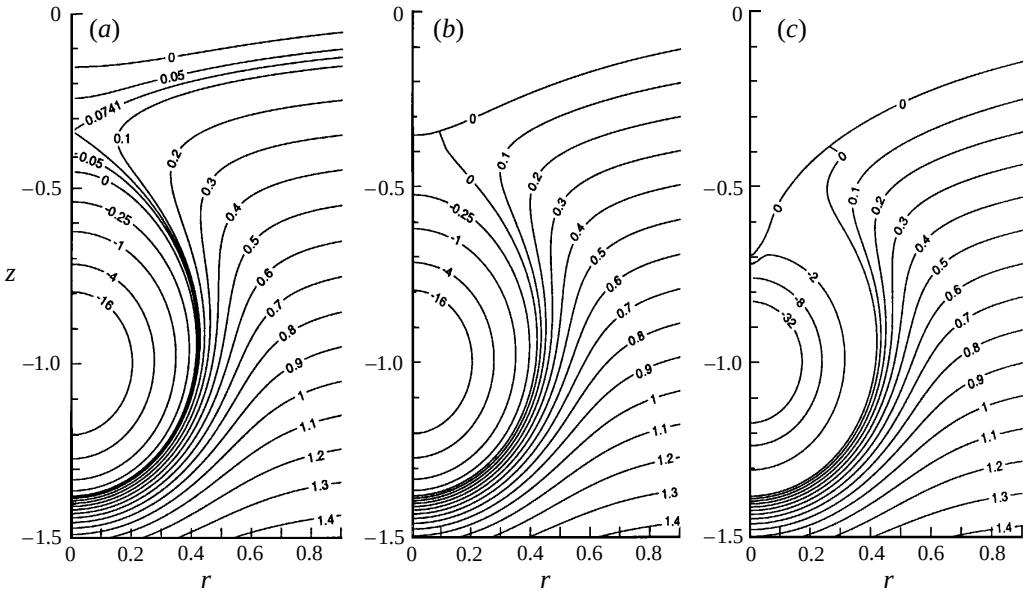

FIGURE 10. Constant-pressure contours for super-critical $\mathscr{F} = 0.24$ at three stages of the evolution: (*a*) $t = 0.288$; (*b*) 0.592; (*c*) 0.828. The vertical and horizontal scales are different.

figure 8*b*), it remains remarkably stable throughout the evolution. Rayleigh–Taylor instability (Taylor 1950) does not obtain in this case because of the non-uniform flow and free-surface deformation. Dagan (1975) analyses the (linearized) stability for the case of non-uniform steady free-surface flow and shows that in addition to Taylor's dynamic condition on the normal (to the free surface) pressure gradient, stability depends also on a kinematic condition regarding the rate of strain of the free surface. Although this result is strictly valid only for the initial (linear) development of instability in steady flows, it shows clearly the favourable/adverse effects of stretching/contracting motions on free-surface stability. These effects are also observed in numerical simulations of nonlinear unsteady motions (e.g. the instability of a collapsing axisymmetric gas bubble, Baker, Meiron & Orszag 1984; but stability for the expanding/rising bubble region of a fluid layer floating on air, Baker *et al.* 1987). In the present case, the stability is a result of the stabilizing effect of the rapid stretching of the free surface near the centre (e.g. figures 9, 10) which dominates the destabilizing effect of the large inward acceleration of the surface. A measure of this stretching is the value of the surface strain rate at the centre, namely, $\phi_{ss}(0,t) \equiv \partial^2/\partial s^2\,\phi(0,t)$, where s is the arclength of the free surface measured from the centre. This strain rate is plotted with the centreline acceleration in figure 8(*b*). We see that as $\ddot{\eta}(0,t)$ decreases to large negative values, ϕ_{ss} undergoes a marked reversal eventually becoming positive and large.

4.3. *Trans-critical regime:* $0.1924 \approx \mathscr{F}_1 < \mathscr{F} < \mathscr{F}_2 \approx 0.1930$

As we pointed out, the sub-critical solution behaviour (with an asymptotic steady state) is suggested at least for small $\mathscr{F}$ from linear theory, while the super-critical solution (with a developing centre dip) can be anticipated from physical arguments at least in the limit of large $\mathscr{F}$. Careful and systematic search of the solution space however reveal clearly a small but distinct trans-critical regime.

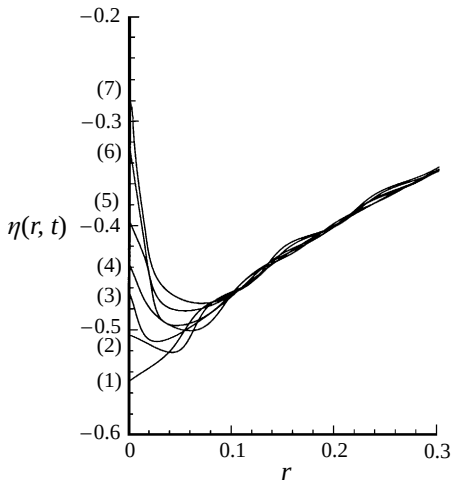

FIGURE 11. Free-surface profiles for trans-critical $\mathscr{F} = 0.1927$ at different times (1) $t = 1.248$; (2) 1.284; (3) 1.304; (4) 1.324; (5) 1.344; (6) 1.364; (7) 1.380. The horizontal and vertical scales are equal (the sink is at $z = -1$).

The solution in this trans-critical regime is characterized by a sharp reversal near the origin of the initially downward motion of the free surface eventually developing into a sharp upward jet immediately above the sink. Similar jets are also often observed when the cavity in a bubble collapses or when steep gravity waves approach a vertical sea-wall or a ship's hull (Longuet-Higgins & Oguz 1997). Figure 11 plots the instantaneous free-surface profiles for a typical trans-critical solution $\mathscr{F} = 0.1927$ during the later stage of the evolution. As in the other two regimes, the free surface drops initially everywhere reaching a minimum depth at the centre. The free surface then rebounds abruptly, starting from the origin outwards, and eventually develops into a sharp upward spike in the centre. Such an upward jet has some resemblance to that observed in Zhou & Graebel (1990) for a tank with small draining rate. In their case, however, the occurrence of such a jet is found to depend on the size of the drain, and as that size decreases to zero the upward jet does not occur even for very small Q (the flow remains 'super-critical' with the formation of a centre dip).

The temporal development and especially the velocity reversal can be best seen in the evolution of the centreline elevation $\eta(0, t)$ plotted in figure 12(a). The surface drops initially reaching a minimal depth of about half the sink submergence at $t \simeq 1.25$ at which point it reverses upwards abruptly. The small kink in the curve after the reversal (at $t \simeq 1.3$) in figure 12(a) is part of the solution and not a numerical artifact as this solution feature remains when spatial/temporal discretizations are substantially refined. We are able to continue the simulation and follow the full development of the upward jet which eventually develops into a centre spike at which point the solution finally fails. The ultimate maximum height of the upward jet is of practical interest and can be estimated from the centreline vertical velocity of the jet after it has developed. From figure 12(a), $W = \dot{\eta}(0, t) \approx 2.5$ after $t \approx 1.33$ when $\eta(0, t) \sim -0.5$. This yields a maximum height of the upward jet of $\sim 0.5W^2 - 0.5 \sim 2.63$ for this case.

The acceleration of the free surface directly above the sink $\ddot{\eta}(0, t)$ is plotted in figure 12(b). Its evolution is quite complex, undergoing altogether three sign changes with a distinct double sign change just prior to the development of the upward jet.

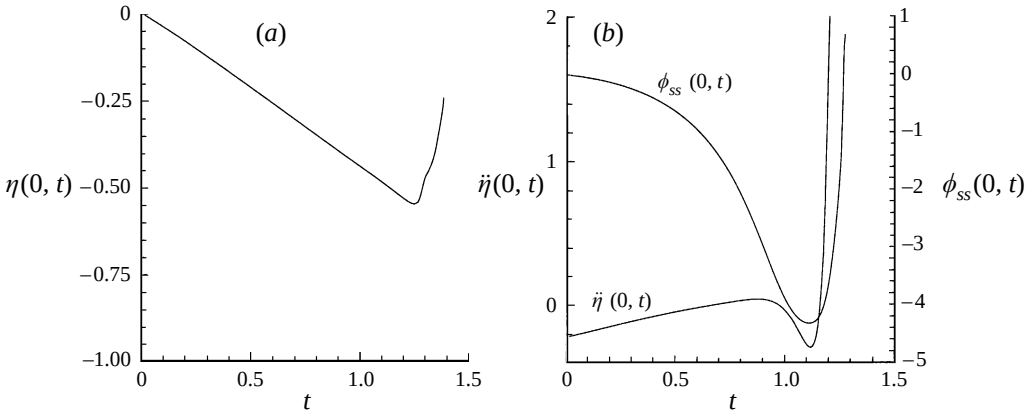

FIGURE 12. Time evolution of the centreline free-surface elevation $\eta(0,t)$, acceleration $\ddot{\eta}(0,t)$ and strain rate $\phi_{ss}(0,t)$ (s is arclength) for trans-critical $\mathscr{F} = 0.1927$.

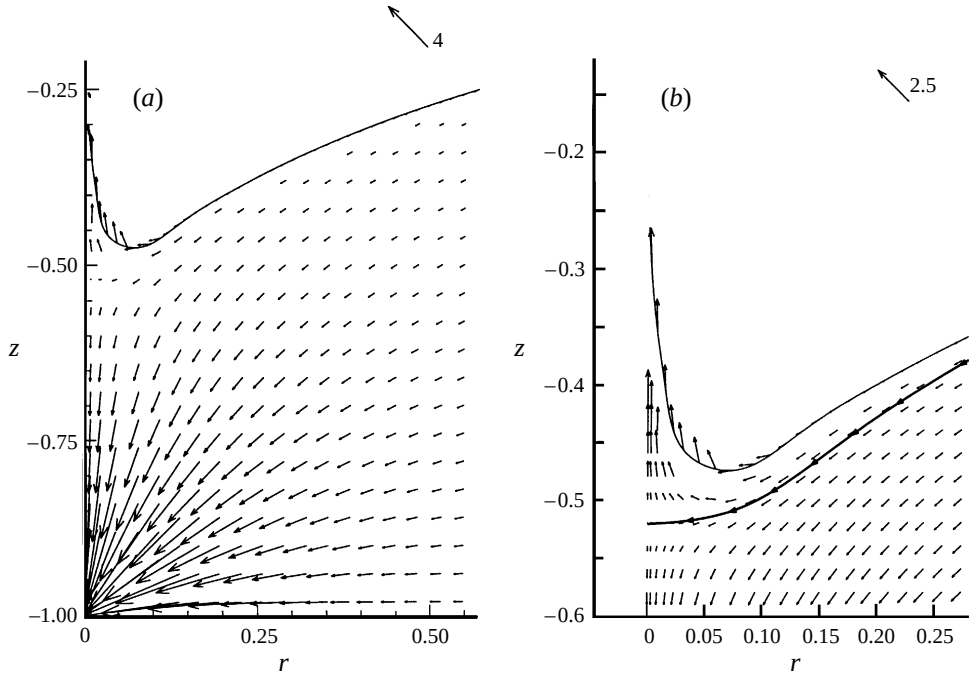

FIGURE 13. Velocity field for trans-critical $\mathscr{F} = 0.1927$ at $t = 1.38$ for (a) 'outer'; and (b) close-up views. In (b) the dividing streamline ending at the stagnation point near $(0, -0.52)$ is also plotted. The sink is at $z = -1$ and the vertical and horizontal scales are equal in each case. Reference vectors are given above.

A plot of the flow field after the free-surface reversal reveals clearly the flow structure. This is shown in figure 13 at $t = 0.84$ which is in the final stage of the upward jet development. The most prominent feature is the presence of a stagnation point above the sink (at $z \sim -0.52$) similar to that in the case of sub-critical withdrawal (cf. figure 6). A dividing streamline emanating from this stagnation point and becoming almost parallel to the free surface some distance away divides the flow field into two regions. In the lower region, the flow converges smoothly towards the

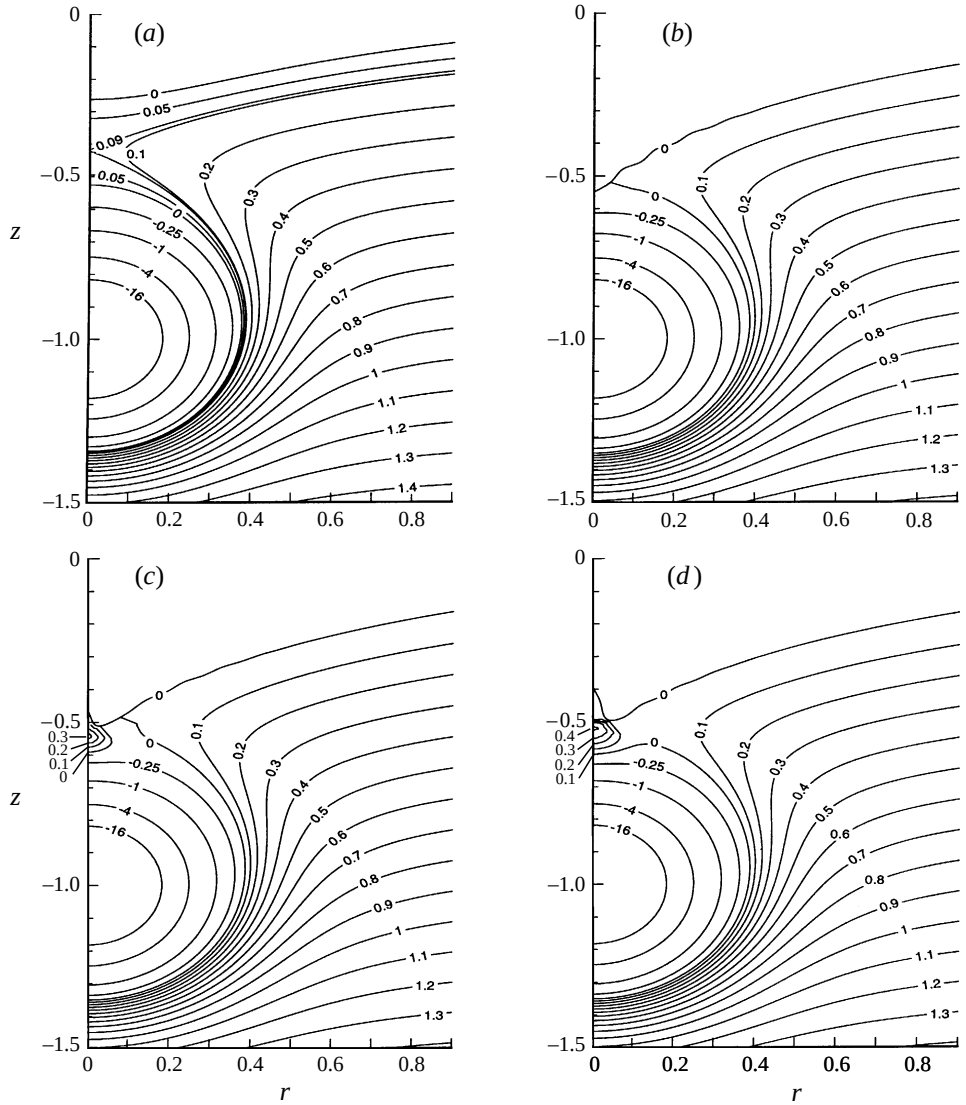

FIGURE 14. Constant-pressure contours for trans-critical $\mathscr{F} = 0.1927$ at four stages of the evolution: (*a*) $t = 0.608$; (*b*) 1.248; (*c*) 1.304; (*d*) 1.344. The vertical and horizontal scales are different.

sink. In the region above the dividing streamline, the velocity is tangent to the free surface (the free surface is streamline-like) some distance away forming a (slightly downward) converging jet-like sheet. As this radial jet converges towards the centre, the velocity is directed upwards over a very small distance, reaching large magnitudes at the origin near the free surface below a sharp upward jet.

To understand the overall evolution, it is again useful to examine the underlying pressure fields. These are plotted at four representative times corresponding to different stages of the development in figure 14. The pressure fields in the early stages are very similar to those for super-critical flow (see figure 10): the presence of an interior zero-pressure contour around the sink (figure 14*a*), which then connects to the free surface eliminating the positive-pressure zone above the sink (figure 14*b*). This (a

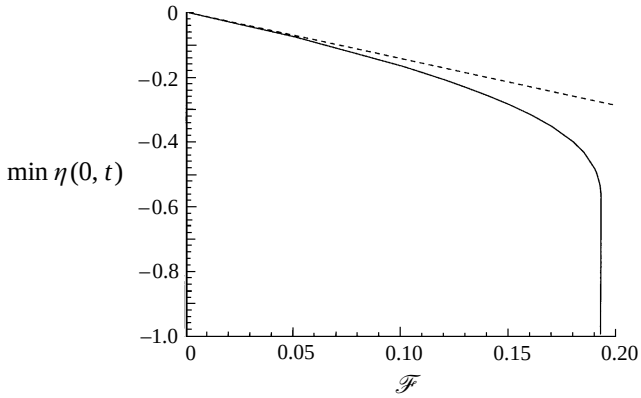

FIGURE 15. Minimum value of the centre surface elevation (over the entire evolution) η_{min} as a function of $\mathscr{F}$. For $\mathscr{F} > \mathscr{F}_2 = 0.1930$, $\eta_{min} = -1$ as the sink is ultimately aerated. Note that $\eta_{min}(\mathscr{F})$ is smooth across the regime transition at $\mathscr{F} = \mathscr{F}_1 = 0.1924$. Dashed line is from linear theory according to (15).

monotonically decreasing pressure from the free surface downwards) is however not a sufficient condition for the subsequent development of a downward dip. As the surrounding fluid converges towards the centre driven by a radial pressure gradient, the sink flux rate in this trans-critical regime is inadequate to draw in the total flow. A stagnation point becomes established above the sink (see figure 13) surrounded by a new (third) zero-pressure contour which also connects to the free surface (figure 14*c*). During the final stage, the zero-pressure contours previously connected to the free surface merge and move under the positive-pressure zone as it strengthens (figure 14*d*). The streamline ending at the stagnation point (see figure 13) now divides the flow, with the converging flow above it directed into an upward jet driven by the large positive pressure at the stagnation point. The trans-critical flow regime is thus seen as one wherein there is a special 'balance' between the radially converging flow initiated by the start-up of the withdrawal and the (constant) flux rate of that withdrawal.

We remark in closing on the 'Taylor' instability of the flow in this regime. As we see from figure 12(*b*), the downward (inward) acceleration of the free surface is never close to the magnitude of gravity (−1 in figure 12*b*) throughout the evolution. Yet, from figures 11 and 14 (especially figure 14*b*), there are distinct signs of a developing instability on the free surface. The instability is thus a result of the negative (contracting) straining of the free surface created by the near-surface radially-converging flow. The straining rate at the centre is plotted with the centreline acceleration in figure 11(*b*). Note that $\phi_{ss}(0,t)$ does not become positive until after $\eta(0,t)$ reverses. It is noteworthy that after the upward jet develops and the centreline strain becomes positive, there are clear indications that the free surface is re-stabilized (compare e.g. the free surface profiles between intermediate and late times, say figures 14(*b*) and 14(*c*); see also figure 11). This is probably the main reason why we are able to continue the numerical simulations well after the (initial) development of instability.

4.4. *Comparison of the different flow regimes*

An interesting result is obtained if we plot the minimum value (over the entire evolution) of the centerline surface elevation, $\eta_{min} \equiv \min \eta(0,t)$, as a function of $\mathscr{F}$ (figure 15). For super-critical $\mathscr{F}$, $\eta_{min} = -1$, as the surface is ultimately drawn into

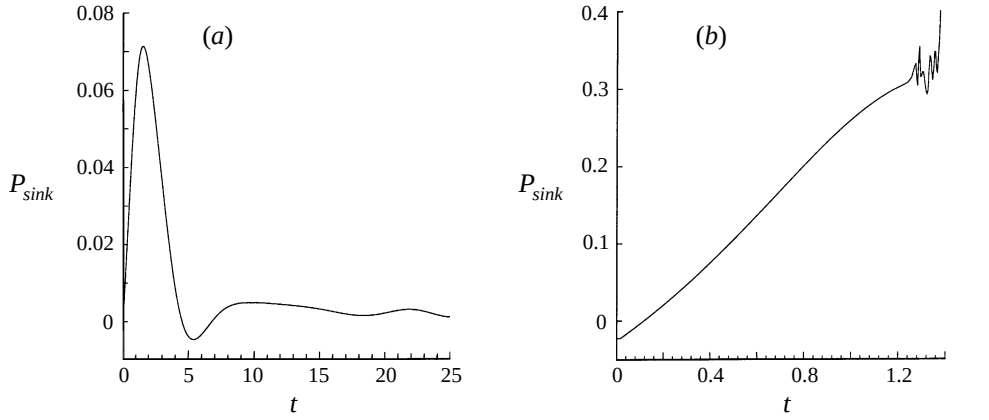

FIGURE 16. Time history of the sink power P_{sink} for (*a*) sub-critical $\mathscr{F} = 0.1$; and (*b*) trans-critical $\mathscr{F} = 0.1927$. Note the different scales in the two cases.

and aerates the sink. For the two non-super-critical regimes $\mathscr{F} < \mathscr{F}_2$, however, we note that $\eta_{min}(\mathscr{F})$ is completely smooth across the regime transition at $\mathscr{F}_1 = 0.1924$. Further analysis reveal that this is in fact also true for the derivative $\eta'_{min}(\mathscr{F})$. The exact explanation for this is unclear. Arguably it should not be surprising that $\eta_{min}(\mathscr{F})$ should behave like a smooth function. That it should be so when the overall solution behaviour changes so dramatically is remarkable. Also plotted in figure 15 is the linearized prediction based on (15) which gives a constant slope for $\eta_{min}(\mathscr{F})$ ($\eta'_{min}(0) \approx -1.466$). This agrees well with the nonlinear result but only for $\mathscr{F}$ very much lower that the critical value $\mathscr{F}_1 \approx 0.1924$.

A practically important quantity for this problem is the power or rate of work done by the sink in the withdrawing process. This is given in (13) (P_{sink} equals twice the quantity expressed therein) and is obtained for different $\mathscr{F}$. Figure 16 shows the typical sink power curves for the sub-critical and trans-critical regimes. For the sub-critical case, the rate of work done by the sink follows closely that of the surface elevation (with an opposite sign), for example at the origin (cf. figure 3), and decays to zero (steady state) after one main oscillation (according to linear theory, in fact, $P_{sink}(t) = -\sqrt{2}\pi\mathscr{F}\,\eta(0, t/\sqrt{2})$). For the trans-critical regime, $P_{sink}(t)$ rises steadily then becomes highly oscillatory as flow reversal occurs. Despite the oscillations, the power equation (13) is satisfied to within $\sim 1\%$ during the entire simulation (cf. §3).

The time history of the power is more varied for super-critical draw-down. Typical results are shown in figure 17. Depending on the value of $\mathscr{F} > \mathscr{F}_2 = 0.1930$, there are three possible sub-regimes for $P_{sink}(t)$: (*a*) $\mathscr{F}_2 < \mathscr{F} < \mathscr{F}_3 \approx 0.21$ – the power rises monotonically throughout, steady at first and then dramatically in the final phase as the surface is drawn into the sink; (*b*) $\mathscr{F}_3 < \mathscr{F} < \mathscr{F}_4 \approx 0.60$ – the power first increases, reaches a maximum and then drops rapidly as the free surface is drawn down; (*c*) $\mathscr{F} > \mathscr{F}_4$ – the power decreases monotonically from its initial value.

It should be noted that P_{sink} is initially negative for this problem for any $\mathscr{F} > 0$. Physically, this means that the sink extracts energy from that (which is unbounded for an infinitesimally small sink) associated with the initial abrupt start-up. Except for trans-critical and the first sub-regime of super-critical flow, $\mathscr{F}_1 < \mathscr{F} < \mathscr{F}_3$, a maximum value of $P_{sink}(t)$ always exists. This is plotted in figure 18 as a function of $\mathscr{F}$. The behaviours of the curves for $\mathscr{F} < \mathscr{F}_1$ and $\mathscr{F} > \mathscr{F}_3$ is qualitatively different and is indicative of the sub-critical to super-critical transition(s).

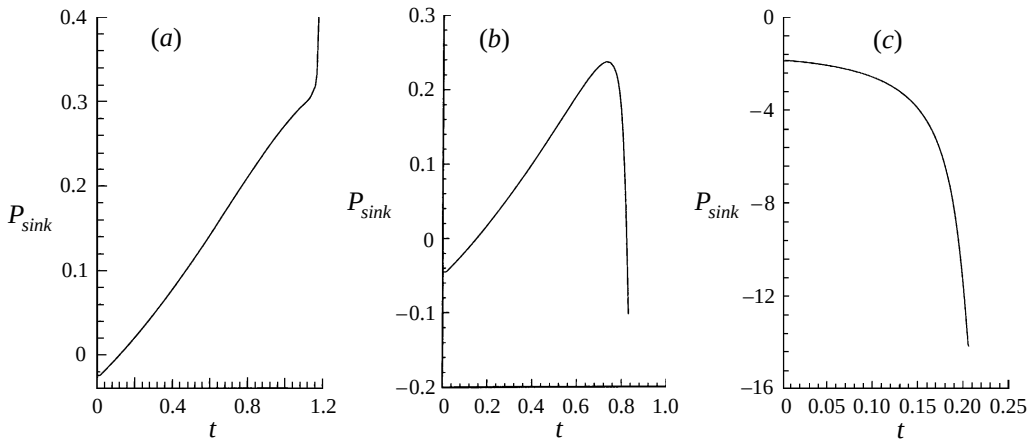

FIGURE 17. Time history of the sink power P_{sink} for super-critical $\mathscr{F} > \mathscr{F}_2 = 0.1930$ withdrawal for (*a*) $\mathscr{F} = 0.1975$; (*b*) $\mathscr{F} = 0.24$; and (*c*) $\mathscr{F} = 0.8$. Note the different scales in the three cases.

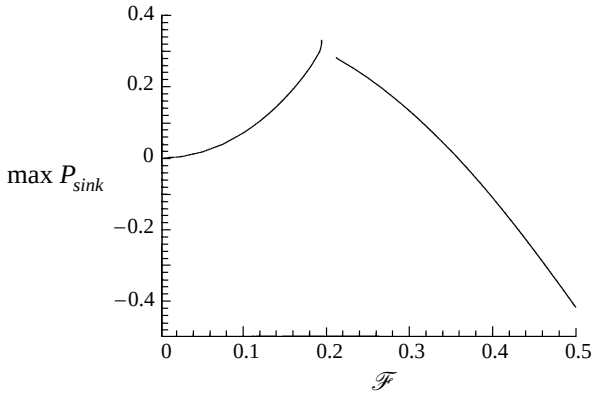

FIGURE 18. Maximum value of the sink input power P_{sink} as a function of $\mathscr{F}$. Note that a maximum value for P_{sink} is well defined only for $\mathscr{F} < \mathscr{F}_1 \approx 0.1924$ and $\mathscr{F} > \mathscr{F}_3 \approx 0.21$.

Another dynamical quantity of practical interest is the (vertical) force on the sink:

$$F_z = -\tfrac{1}{3}\rho Q \frac{\partial}{\partial z}\left[\phi - \frac{Q}{4\pi|\boldsymbol{x}-\boldsymbol{x}_{sink}|}\right]_{\boldsymbol{x}_{sink}} \tag{16}$$

$$= \rho \iint_{\overline{F}} \left(\tfrac{1}{2}|\nabla\phi|^2 n_z - \frac{\partial\phi}{\partial z}\frac{\partial\phi}{\partial n}\right) \mathrm{d}S$$
$$-\rho \iint_{M} \frac{\partial\phi}{\partial r}\frac{\partial\phi}{\partial z}\mathrm{d}S - \rho \iint_{B} \tfrac{1}{2}|\nabla\phi|^2 \mathrm{d}S - \tfrac{4}{3}\rho Q \frac{\partial}{\partial z}\left[\phi - \frac{Q}{4\pi|\boldsymbol{x}-\boldsymbol{x}_{sink}|}\right]_{\boldsymbol{x}_{sink}}. \tag{17}$$

Equation (16) is simply 1/3 the localized Lagally force (Milne-Thomson 1968), while (17) provides the boundary-integral formula obtained by considering momentum conservation inside $S(t)$. These equivalent expressions provide a further check of the numerics – in all our simulations, F_z using either formula differs by less than $O(1\%)$. Furthermore, in all our results, the term in (17) which accounts for the (computational) bottom at finite depth is at least two orders of magnitude smaller than the remaining terms indicating that the chosen $H = 6$ is sufficient.

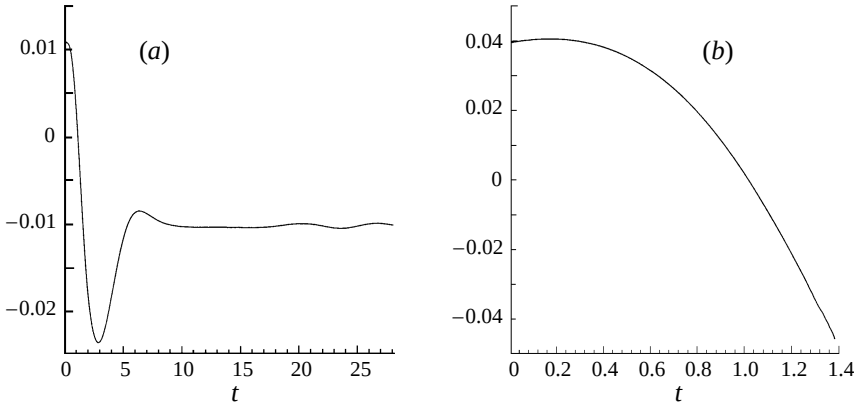

FIGURE 19. Time history of the vertical force on the sink for (*a*) sub-critical $\mathscr{F} = 0.1$; and (*b*) trans-critical $\mathscr{F} = 0.1927$. Note the different scales in the two cases.

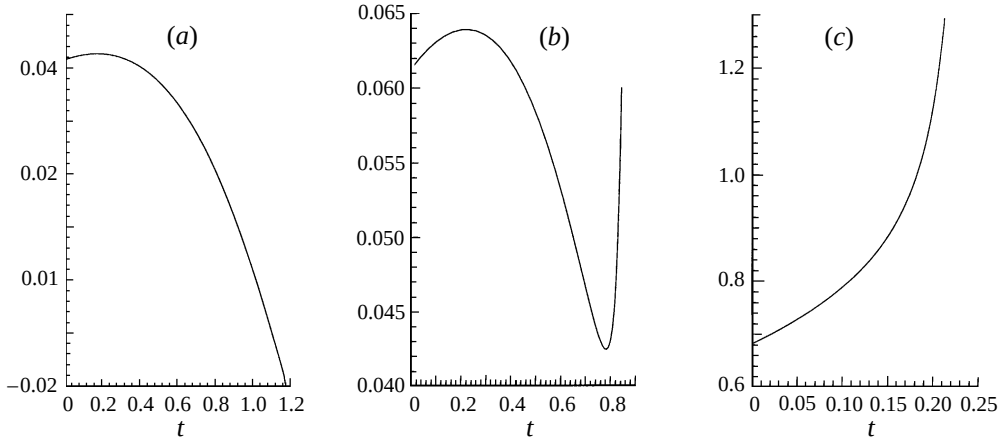

FIGURE 20. Time history of the vertical force on the sink for super-critical $\mathscr{F} > \mathscr{F}_2 = 0.1930$ withdrawal for (*a*) $\mathscr{F} = 0.1975$; (*b*) $\mathscr{F} = 0.24$; and (*c*) $\mathscr{F} = 0.8$. Note the different scales in the three cases.

Figure 19 shows $F_z(t)$ for typical sub- and trans-critical withdrawals. As expected, both curves start with positive values (according to linearized theory $F_z(0) = \pi\mathscr{F}^2/3$). The former (figure 19*a*) decreases from that initial value, then undergoes the characteristic oscillation and asymptotic decay (cf. figure 3 for example). For the trans-critical case, F_z initially increases, reaching a maximum and then decreases monotonically eventually becoming negative before the free surface reverses direction.

The super-critical F_z again exhibits qualitatively different behaviour in three subregimes (figure 20): (*a*) $\mathscr{F}_2 < \mathscr{F} < \mathscr{F}_3$ – similar to the trans-critical case, monotonic decrease after an initial period of slight increase; (*b*) $\mathscr{F}_3 < \mathscr{F} < \mathscr{F}'_4$ – F_z remains positive throughout, first reaching a (local) maximum, decreases to a positive minimum value, then reverses direction again to increase monotonically; (*c*) $\mathscr{F} > \mathscr{F}'_4$ – the vertical force rises monotonically from its initial (positive) value. Note that $\mathscr{F}'_4 \simeq 0.35$ is much lower than $\mathscr{F}_4$ for the power.

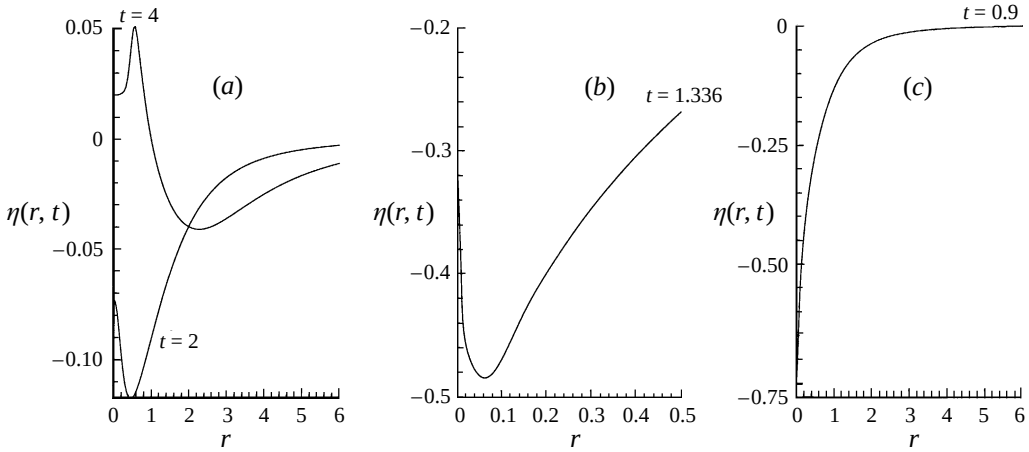

FIGURE 21. Typical free-surface profiles for a ramp-like start-up of the sink, $\delta t = 0.06$ for (*a*) sub-critical $\mathscr{F} = 0.1$; (*b*) trans-critical $\mathscr{F} = 0.1927$; and (*c*) super-critical $\mathscr{F} = 0.24$. Note the different horizontal and vertical scales.

We remark in closing that all results so far are for an abrupt start-up of the sink. It is reasonable to ask whether our conclusions are sensitive to the initial behaviour of the drain rate function, say $q(t)$, in a more gradual start-up (e.g. Zhou & Graebel 1992). In particular, it is important to show that a trans-critical regime still exists in that case. From the concluding discussions in §4.3, it is seen that the upward jet is a result of a special balance between the initial draw-in and the constant flux rate of the sink. It is reasonable then to argue that a range of trans-critical Q would exist for a slightly more gradual start-up, although the precise values of $\mathscr{F}_1$ and $\mathscr{F}_2$ bounding this regime must be sensitive to $q(t)$. To verify this, we introduce another parameter into the problem, namely the start-up time scale δt, and consider ramp-like drain rate functions of the form

$$q(t) = \begin{cases} Qt/\delta t, & 0 \leqslant t \leqslant \delta t \\ Q, & t \geqslant \delta t. \end{cases} \tag{18}$$

We incrementally increase δt, and for each value again perform a systematic search of $\mathscr{F}$. The volume of results is fairly large and can be found in Xue (1997). The important conclusion is that for sufficiently small $\delta t \lesssim 0.06$, the three distinct regimes corresponding to the qualitatively different sub-, trans-, and super-critical flows still obtain. For larger values of δt, the trans-critical regime disappears. As expected, a more gradual start-up of the flow is less conducive to the development of the trans-critical upward spike and the super-critical collapse. The values of the critical Froude numbers $\mathscr{F}_1$ and $\mathscr{F}_2$ are therefore generally higher for smoother starting conditions. The critical values of $\mathscr{F}_1$ and $\mathscr{F}_2$ we report for impulsive withdrawal are thus the minimum values for this problem. This should be noted in comparisons to physical experiments. Figure 21 shows typical free-surface profiles for the case of $\delta = 0.06$ for the three regimes respectively. The qualitative features are still quite similar to those for abrupt start-up.

5. Summary and discussion

We consider the initial-boundary-value problem of the withdrawal of fluid by a (point) sink submerged a distance h (initially) under a free surface in otherwise

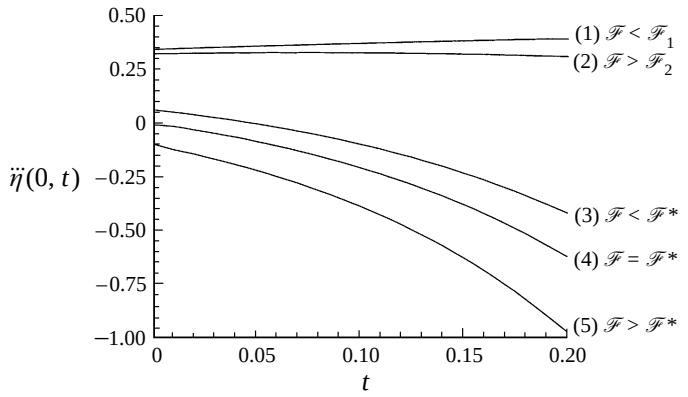

FIGURE 22. Third-order time derivative of the free-surface elevation at $r = 0$, $\partial^3/\partial t^3\, \eta(0, t)$, for different Froude numbers (1) $\mathscr{F} = 0.10$; (2) 0.20; (3) 0.25; (4) $15^{-1/2}$; (5) 0.27.

unbounded fluid. In the context of potential flow and impulsive start reaching a constant volume flow rate Q, the problem, under gravitational acceleration g, is governed by a single physical parameter, the Froude number $\mathscr{F} \equiv Q/4\pi(gh^5)^{1/2}$. We assume axisymmetry and perform fully nonlinear numerical computations using a special far-field matching technique to allow long-time simulations. The complete solution of the problem is mapped systematically varying $\mathscr{F}$ to reveal three distinct flow regimes: (i) sub-critical regime, $\mathscr{F} < \mathscr{F}_1$ – damped wave-like flow with asymptotic steady state; (ii) trans-critical regime, $\mathscr{F}_1 < \mathscr{F} < \mathscr{F}_2$ – flow reversal developing into a sharp upward jet; and (iii) super-critical regime, $\mathscr{F} > \mathscr{F}_2$ – rapid jet-like collapse of the free surface. For impulsive start-up, the critical Froude numbers are found to be $\mathscr{F}_1 \approx 0.1924$ and $\mathscr{F}_2 \approx 0.1930$.

It is instructive to compare our results to that of Miloh & Tyvand (1993) who obtain a value of the critical Froude number of $\mathscr{F} = \mathscr{F}^* = 15^{-1/2} \simeq 0.258$ for this problem based on a small-time perturbation analysis. Presumably, for $\mathscr{F} > \mathscr{F}^*$, the free surface will (eventually) collapse into the sink and steady state is not possible. We note that $\mathscr{F}^*$ is appreciably greater than $\mathscr{F}_2$ so that while the small-time expansion does not contradict the present results, its prediction of $\mathscr{F}^*$ can be regarded only as a weak upper bound. Miloh & Tyvand (1993) obtain $\mathscr{F}^*$ based on an argument of balance between nonlinear and gravity effects at $r = 0$ (and $t = 0$) which is equivalent to the vanishing of the term $\ddot{\eta}\,(0,0) \equiv \partial^3/\partial t^3\, \eta(0,0)$. Not surprisingly, our computational results agree with theirs (only) for very small t. Figure 22 plots our computed $\ddot{\eta}\,(0,t)$ for different $\mathscr{F}$. At $t = 0$, we confirm that $\mathscr{F} = \mathscr{F}^* \simeq 0.258$ indeed divides positive and negatives of $\ddot{\eta}\,(0,0)$. For $\mathscr{F} > \mathscr{F}^*$, $\ddot{\eta}\,(0,t)$ remains negative with increasing t, but for $\mathscr{F}$ close to and less than $\mathscr{F}^*$, $\ddot{\eta}\,(0,t)$ changes sign from positive to negative after a very short time (cf. curve (3) in figure 22). This rapid variation with time explains the difficulty of using an expansion in time around $t = 0$ to predict the ultimate fate of the evolution.

Our prediction of a sub-critical asymptotic steady state may also be compared with Forbes & Hocking (1990)'s finding of steady-state solutions for sufficiently small $\mathscr{F}$. Our critical value of $\mathscr{F} < \mathscr{F}_1 \approx 0.1924$ is however substantially lower than their value of $\mathscr{F} < \mathscr{F}^\dagger = 0.509$ for steady (time-independent) solutions. The relationship between the asymptotic steady state in an initial-value problem as in the present work and the solution of the boundary-value problem where steady state is assumed as in Forbes & Hocking (1990) cannot be established in general. This is obviously not

possible for $\mathscr{F}_1 < \mathscr{F} < \mathscr{F}^\dagger$ since such solutions exist only for the latter. Even for $\mathscr{F} < \mathscr{F}_1$, however, meaningful direct comparisons cannot be made (the lowest $\mathscr{F}$ for which Forbes & Hocking 1990 show results is in fact greater than $\mathscr{F}_1$).

A problem closely related to the present one is the drainage of a circular tank from a hole in the middle of the bottom. Lubin & Springer (1967) study this problem experimentally and observe that the critical height at which there is dip formation is independent of the initial height and during which the volume flow rate can be considered constant. Based on this observation, they assume quasi-steady flow at that instant and perform a very simple hydraulic analysis using the Bernoulli equation. This crude calculation yields a critical Froude number $\mathscr{F}^\ddagger = [2^7/5^5]^{1/2} \simeq 0.202$ for the initiation of the (super-critical) dip. This value is also in good agreement with their experimental measurements. While the assumptions and certain aspects of the simple analysis of Lubin & Springer (1967) can be questioned, it is quite remarkable that their value of 0.202 is within 5% of our predicted value of $\mathscr{F}_2 \approx 0.1930$.

A difficulty of comparing the problem of drainage from a circular tank with the present one in unbounded fluid is that in the former case the average depth varies with time (and the free surface is not horizontal when critical depth is reached) so that a well-defined/precise Froude number based on height cannot be established. This precludes more direct comparisons, for example, with the simulations of Zhou & Graebel (1990) for the circular tank problem (their problem also contains additional parameters associated with the tank radius and the radius of the drain). Nevertheless, approximate comparisons can be made if we make reasonable estimates of the equivalent critical height, $\hat{h}$ say, based on the evolving free-surface profiles. Defining $\hat{h}$ as the height of the free surface on the sidewall at the instant when the free-surface dip just begins to develop, and accounting for the effect of finite radius (cf. Miloh & Tyvand 1993), we obtain from Zhou & Graebel (1990) equivalent critical Froude number values for the development of a centre dip of $\hat{\mathscr{F}}$ in the ranges 0.163–0.202 and 0.202–0.232 (from their figures 2 and 3 respectively). These values are still in reasonable agreement with the critical value for our problem of $\mathscr{F}_2 \approx 0.1930$.

Finally we note that the problem we consider here of a fixed sink, impulsive start, and constant volume flux rate, is a specialized case. The computational method we present is general and can be extended in straightforward ways to account for effects such as a sink in motion, time-varying drain rates, and the presence of boundaries.

This work is supported financially by the Office of Naval Research. We thank Professor T. Miloh for helpful discussions.

REFERENCES

Baker, G. R, McCrory, R. L., Verdon, C. P. & Orszag, S. A. 1987 Rayleigh–Taylor instability of fluid layers. *J. Fluid Mech.* **178**, 161.

Baker, G. R, Meiron, D. I. & Orszag, S. A. 1984 Boundary integral methods for axisymmetric and three-dimensional Rayleigh–Taylor instability problems. *Physica* **12D**, 19.

Collings, I. L. 1986 Two infinite-Froude-number cusped free-surface flows due to a submerged line source or sink. *J. Austral. Math. Soc.* B **28**, 260.

Dagan, G. 1975 Taylor instability of a non-uniform free-surface flow. *J. Fluid Mech.* **67**, 113.

Dommermuth, D. G. & Yue, D. K. P. 1987 Numerical simulations of nonlinear axisymmetric flows with a free surface. *J. Fluid Mech.* **178**, 195.

Forbes, L. K. & Hocking, G. C. 1990 Flow caused by a point sink in a fluid having a free surface. *J. Austral. Math. Soc.* B **32**, 231.

Hocking G. C. 1985 Cusp-like free-surface flows due to a submerged source or sink in the presence of a flat or sloping bottom. *J. Austral. Math. Soc.* B **26**, 470.

Hocking, G. C. 1988 Infinite Froude number solutions to the problem of a submerged source or sink. *J. Austral. Math. Soc.* B **29**, 401.

Hocking, G. C. & Forbes, L. K. 1991 A note on the flow induced by a line sink beneath a free surface. *J. Austral. Math. Soc.* B **32**, 251.

King, A. C. & Bloor, M. I. G. 1988 A note on the free surface induced by a submerged source at infinite Froude number. *J. Austral. Math. Soc.* B **30**, 147.

Longuet-Higgins, M. S. & Oguz, H. N. 1997 Critical jets in surface waves and collapsing cavities. *Phil. Trans. R. Soc. Lond.* A **355**, 625.

Lubin, B. T. & Springer, G. S. 1967 The formation of a dip on the surface of a liquid draining from a tank. *J. Fluid Mech.* **29**, 385.

Mekias, H. & Vanden-Broeck, J.-M. 1989 Supercritical free-surface flow with a stagnation point due to a submerged source. *Phys. Fluids* A **1**, 1694.

Mekias, H. & Vanden-Broeck, J.-M. 1991 Subcritical flow with a stagnation point due to a source beneath a free surface. *Phys. Fluids* A **3**, 2652.

Mekias, H. & Vanden-Broeck, J.-M. 1993 Free-surface flow due to a source submerged in fluid of infinite depth with two stagnant regions. *J. Austral. Math. Soc.* B **34**, 368.

Milne-Thomson, L. M. 1968 *Theoretical Hydrodynamics*, 5th edn. Macmillan.

Miloh, T. & Tyvand, P. A. 1993 Nonlinear transient free-surface flow and dip formation due to a point sink. *Phys. Fluids* A **5**, 1368.

Monismith, S. G., McDonald, N. R. & Imberger, J. 1993 Axisymmetric selective withdrawal in a rotating stratified fluid. *J. Fluid Mech.* **249**, 287.

Peregrine, D. H. 1972 A line source beneath a free surface. *Mathematics Research Center, Univ. Wisconsin, Technical Summary Rep.* 1248.

Sahin, I. & Magnuson, A. H. 1984 A numerical method for the solution of a line source under a free surface. *Ocean Engng.* **11**, 451.

Taylor, G. 1950 The instability of liquid surfaces when accelerated in a direction perpendicular to their planes. I. *Proc. R. Soc. Lond.* A **201**, 192.

Tuck, O. E. & Vanden-Broeck, J.-M. 1984 A cusp-like free-surface flow due to a submerged source or sink. *J. Austral. Math. Soc.* B **25**, 443.

Tyvand, P. A. 1992 Unsteady free-surface flow due to a line source. *Phys. Fluids* A **4**, 671.

Vanden-Broeck, J.-M. & Keller, J. B. 1987 Free surface flow due to a sink. *J. Fluid Mech.* **175**, 109.

Vanden-Broeck, J.-M., Schwartz, L. W. & Tuck, O. E. 1987 Divergent low-Froude-number series expansion of nonlinear free-surface flow problems. *Proc. R. Soc. Lond.* A **361**, 207.

Wehausen, J. V. & Laitone, E. V. 1960 Surface waves. In *Encyclopedia of Physics*. Springer.

Xue, M. 1997 Three-dimensional fully-nonlinear simulations of waves and wave body interactions. PhD thesis, Massachusetts Institute of Technology, Cambridge, Massachusetts.

Zhou, Q. N. & Graebel, W. P. 1990 Axisymmetric draining of a cylindrical tank with a free surface. *J. Fluid Mech.* **221**, 511.

Zhou, Q. N. & Graebel, W. P. 1992 Free-surface Oscillations in a slowly draining tank. *Trans. ASME*: *J. Appl. Mech.* **59**, 438.